

Dropwise Condensation on Superhydrophobic Microporous Wick Structures

Sean H. Hoenig

Advanced Cooling Technologies, Inc.,
1046 New Holland Avenue,
Lancaster, PA 17601
e-mail: Sean.Hoenig@1-ACT.com

Richard W. Bonner III

Advanced Cooling Technologies, Inc.,
1046 New Holland Avenue,
Lancaster, PA 17601
e-mail: Richard.Bonner@1-ACT.com

Previous research in dropwise condensation (DWC) on rough microtextured superhydrophobic surfaces has demonstrated evidence of high heat transfer enhancement compared to smooth hydrophobic surfaces. In this study, we experimentally investigate the use of microporous sintered copper powder on copper substrates coated with a thiol-based self-assembled monolayer to attain enhanced DWC for steam in a custom condensation chamber. Although microtextured superhydrophobic surfaces have shown advantageous droplet growth dynamics, precise heat transfer measurements are underdeveloped at high heat flux. Sintered copper powder diameters from 4 μm to 119 μm were used to investigate particle size effects on heat transfer. As powder diameter decreased, competing physical factors led to improved thermal performance. At consistent operating conditions, we experimentally demonstrated a 23% improvement in the local condensation heat transfer coefficient for a superhydrophobic 4 μm diameter microporous copper powder surface compared to a smooth hydrophobic copper surface. For the smallest powders observed, this improvement is primarily attributed to the reduction in contact angle hysteresis as evidenced by the decrease in departing droplet size. Interestingly, the contact angle hysteresis of sessile water droplets measured in air is in contradiction with the departing droplet size observations made during condensation of saturated steam. It is evident that the specific design of textured superhydrophobic surfaces has profound implications for enhanced condensation in high heat flux applications.

[DOI: 10.1115/1.4038854]

Keywords: dropwise condensation, superhydrophobicity, microporous wick structures

Introduction

Dropwise condensation on textured nonwetting surfaces has vast applications in two-phase thermal management technologies, including power plant condensers, vapor chambers [1], and heat pipes. High heat transfer enhancement using dropwise condensation (DWC) has been of interest since the earliest published work in 1930, which reported an order of magnitude higher heat transfer coefficient compared to filmwise condensation for comparable conditions [2]. Although there are a multitude of different coating mechanisms to generate ultra-low surface energy, many issues remain to create a consistent, practical surface for industrial use. These issues include poor coating lifetime [3], constriction resistance for low thermally conductive materials [4], and high coating costs [5]. In spite of these issues, various superhydrophobic micro/nanotextured structures have garnered close attention in recent years with respect to modeling and experimental research.

To determine an appropriately textured surface through modeling, Patankar [6,7] demonstrated the need for multiple roughness structures to mimic the microstructure of superhydrophobic lotus leaves. These slender pillars help amplify the apparent contact angle to form a composite drop that can easily depart from the surface. The facilitation of droplet roll-off is the key feature of using long slender pillars as textured structures. Kim and Kim [8] developed a single droplet model that demonstrated the reduction of the minimum droplet size as contact angle increased and captured the resulting increase in heat transfer efficiency. Mendoza et al. [9] additionally discovered a theoretical upper bound to dropwise condensation heat transfer performance. For droplet diameters smaller than 10 μm , the trend of increasing heat transfer coefficient with decreasing mean droplet size diminishes. Beaini et al.

[10] created a tool for understanding optimal micro/nanoscale pillared surfaces for DWC. The results demonstrated that the droplet growth rate on textured surfaces is consistently worse than a smooth surface. A small pillar diameter and height can closely emulate a smooth surface, but the pillar resistance dominates even with varying droplet radius.

With several modeling efforts characterizing the supposed effects of micro/nanotextured structures, several experimental studies have been conducted to challenge these models. Dietz et al. [11] revealed the potential for greater heat transfer enhancement using textured superhydrophobic nanostructures due to the small size of departing droplets (<10 μm). Rykaczewski et al. [12–15] demonstrated the need to use micro/nano surface features to confine droplet formation diameters to sub-10 μm . During coalescence, larger diameter primary drops can actively contribute to sweeping smaller droplets to achieve higher departure rates. The nature of nonwetting states (Cassie or Wenzel) [16] on textured superhydrophobic surfaces also contributes to varying results. Narhe and Beysens [17,18] determined there is a trade-off for textured surfaces between having high surface contact for a droplet in a Wenzel state or high mobility in a Cassie state for heat transfer efficiency. Two-tiered roughness structures [19] have additionally demonstrated sustained Cassie states for small droplet sizes.

In this study, the local condensation heat transfer coefficient is evaluated for superhydrophobic microporous sintered copper powder structures, which extends the research of enhanced filmwise condensation using hydrophilic microporous sintered copper powder [20,21]. This effort is to specifically quantify the extent of improvement in heat transfer efficiency for dropwise condensation on variably sized microporous copper wick monolayers and discuss the interface droplet effects of microtextured superhydrophobic surfaces. Microporous copper wick structures are widely used in heat pipe and vapor chamber designs [22] to transport condensate back to the evaporator section. Many studies regarding heat pipes have been completed to determine optimal permeability and

Contributed by the Heat Transfer Division of ASME for publication in the JOURNAL OF HEAT TRANSFER. Manuscript received April 28, 2017; final manuscript received December 6, 2017; published online April 6, 2018. Assoc. Editor: Gennady Ziskind.

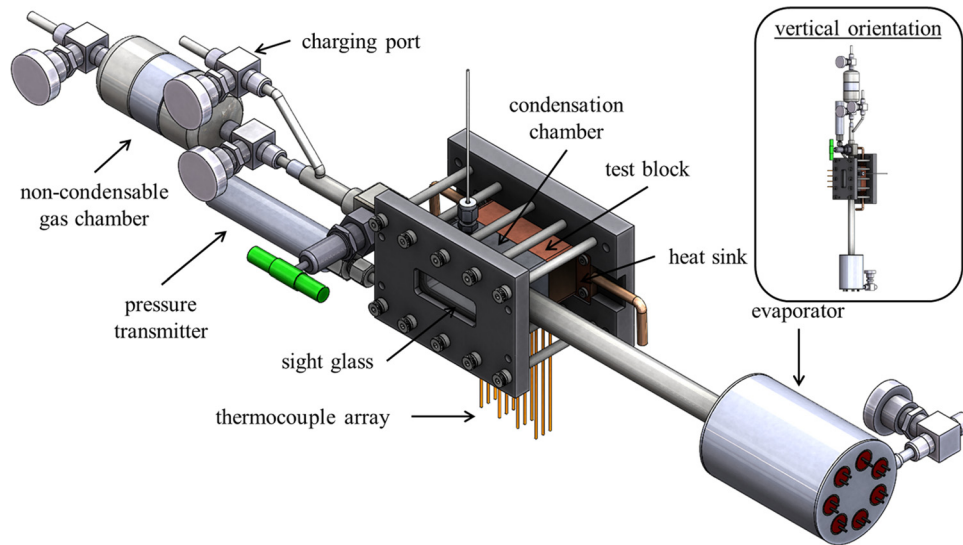


Fig. 1 The test setup demonstrated in SOLIDWORKS in an isometric orientation. The actual orientation is vertical with the evaporator below the condensation chamber. The true orientation is represented in the inset image.

performance using modulated wick structures for evaporation [23–25]. Additional research has examined the visual droplet morphology benefits of nanostructured wick substrates [26]. This is the first comprehensive study to measure and understand the condensation heat transfer enhancement using superhydrophobic microporous copper powder wick structures sintered on copper substrates.

Experimental

Test samples were machined out of commercially available copper alloy 101 to the specifications of the experimental setup. Figures 1 and 2 provide an in-depth look at the details of the experimental apparatus, which is oriented vertically. The active condensing surface is a 5.59 cm × 2.03 cm area centered in the test block. Figure 3 demonstrates the test blocks used for a smooth and textured surface as well as an example scanning electron microscope (SEM) image of the type of monolayer observed. The copper surfaces were first prepared using 1200 grit sandpaper to create a smooth finish and then cleaned with acetone. Microporous copper powder (ACuPowder) was then applied to the test surface to create a monolayer structure. This was done first through the application of a thin layer of Nicrobraz (Wall Colmonoy). The test blocks were then sintered to 975 °C in a hydrogen furnace. The self-assembled monolayer was created using a 5 mM solution of 1*H*,1*H*,2*H*,2*H*-perfluorodecanethiol (Sigma-Aldrich) dissolved in 2-propanol (Sigma-Aldrich, St. Louis, MO). The test blocks were submerged in a sealed bath of the self-assembled monolayer solution for a 24 h period and subsequently dried with dry nitrogen gas. A graphic of superhydrophobic self-assembled monolayers deposited on a sintered microporous copper powder monolayer is shown in Fig. 4. The term monolayer is used to describe the ideal application of powder to the surface; although, there is no consistent one layer of powder in actual use. Each sample was then tested in the experimental apparatus using de-ionized water, which was injected following the use of a vacuum pump to evacuate the system. The absolute pressure for each experimental test was held between 222.49 and 244.69 kPa, which corresponds to a saturated vapor temperature of 105–110 °C. This pressure operating range was chosen to maintain a slightly higher saturated pressure than atmospheric conditions to prevent noncondensable gas (NCG) in leak. During testing, the NCG collection chamber was used to collect NCG and then purge the condensation chamber of any internal NCG buildup. To evaluate the surface temperature of the

substrate for heat transfer calculations, a thermocouple array was used for interpolation. Thermal paste was used to ensure precise thermal coupling of the thermocouples to the thermocouple wells. Results were collected over a range of heat flux data by varying the subsequent cartridge heater input and water chiller output. A transparent sight glass was incorporated to observe the dropwise condensation phenomenon.

Conduction calorimetry was used to calculate heat flux and extrapolate the surface temperature during dropwise condensation. Temperature measurements were acquired at several known locations within the copper test samples. Linear regression was then used to determine the thermal gradients across the block and

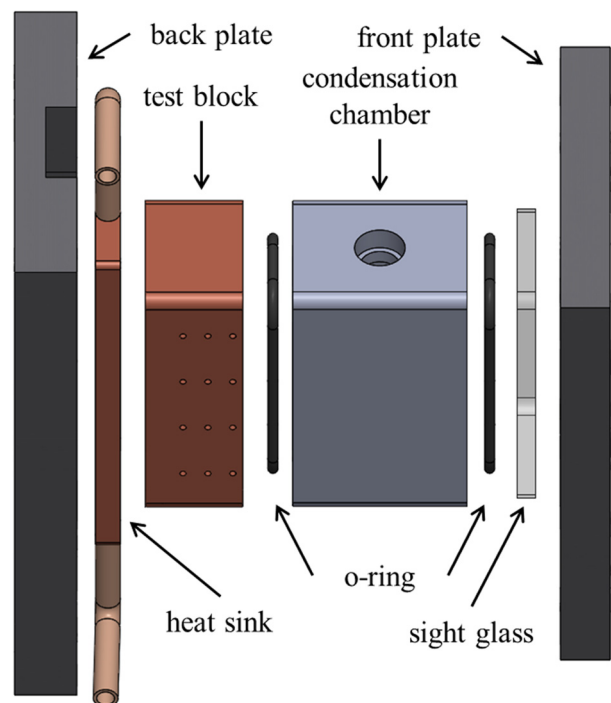


Fig. 2 Exploded view of the condensation chamber and its associated components in SOLIDWORKS demonstrate its functionality

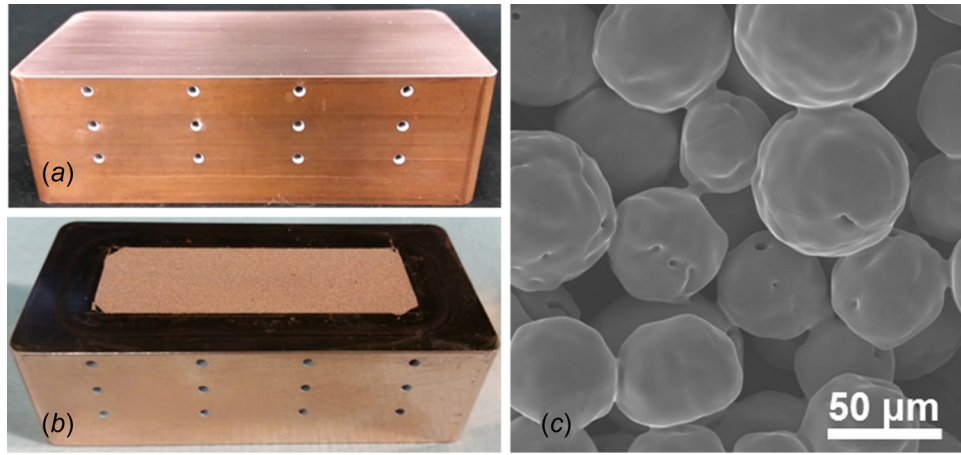


Fig. 3 A smooth copper surface (a) is compared with a microporous copper powder wick sintered to a copper substrate (b). Image (c) is SEM for a 61 μm average diameter powder sample.

extrapolate the surface temperature during dropwise condensation. Heat flux through the block was calculated using Fourier's Law, shown in Eq. (1). The experimental dropwise condensation heat transfer coefficient was calculated using the measured saturated vapor temperature of the condensing steam and Newton's Law of Cooling, shown in Eq. (2). A simplified expression for calculating the dropwise condensation heat transfer coefficient from these measurements is shown in Eq. (3)

$$q'' = k_s \frac{dT}{dx} \quad (1)$$

$$q'' = h_l(T_v - T_s) \quad (2)$$

$$h_l = \frac{k_s \frac{dT}{dx}}{T_v - T_s} \quad (3)$$

Results

Surface Characterization. An experimental trade study was performed where the particle size of microporous sintered copper

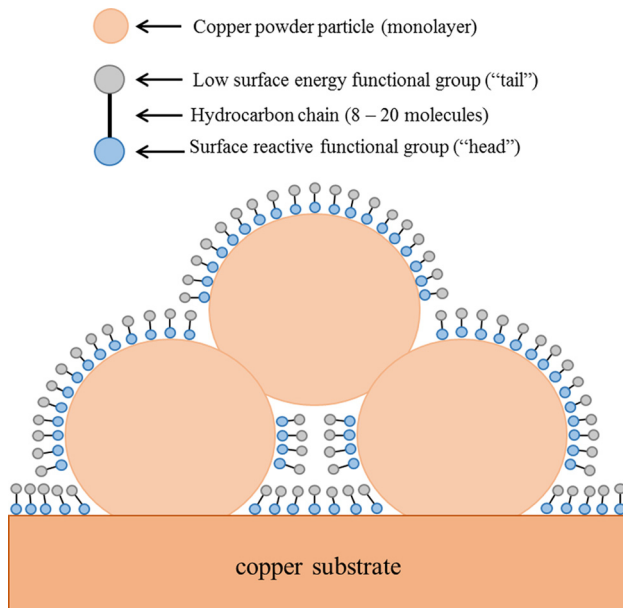


Fig. 4 Self-assembled monolayer coating deposited on a sintered microporous copper powder monolayer and copper substrate

powder was varied in order to evaluate their potential for heat transfer improvement in dropwise condensation. The different copper powders used are shown in Table 1, which additionally includes the advancing and receding contact angles observed in air for sessile water droplets deposited on the surfaces. Visual representation of the advancing contact angle data is demonstrated in Fig. 5. It is clear that the advancing contact angle for a smooth copper surface is only marginally hydrophobic at approximately 91 deg. As roughness is introduced on the copper surface in the form of increasingly larger copper powder monolayers, the advancing contact angle becomes superhydrophobic and greater than 140 deg for all samples except for the smallest powder size (4 μm). The implication here is that this microporous copper powder monolayer more closely emulates a smooth surface than the other roughness induced structures fabricated with larger sized powders. This additionally is demonstrated with the small contact angle hysteresis observed for the 4 μm powder sample relative to the larger sized powders. The analytical importance of these observations becomes clearer as the heat transfer data and reported departing droplet sizes during condensation are analyzed.

Thermal Performance Evaluation. All measured heat transfer results from this effort are found in Fig. 6, which shows the local vapor-to-surface temperature difference (ΔT) as a function of the local condensation heat flux (q''). The results for a smooth hydrophobic copper surface represent a baseline comparison for thermal performance. The additional data from Stylianou and Rose [27] are used as validation of the experimental process for the newly acquired dropwise condensation thermal performance measurements. Both sets of data are for a smooth hydrophobic copper surface tested at comparable experimental conditions. The measured data from Stylianou ($h_l = 171 \pm 10 \text{ kW/m}^2 \text{ K}$) are consistent with the newly acquired data ($h_l = 156 \pm 3 \text{ kW/m}^2 \text{ K}$) for a smooth hydrophobic copper surface in the appropriate data range. The plot of experimental data for ΔT versus heat flux for the different powder and smooth surfaces shows a generally linear trend, indicating a constant heat transfer coefficient as a function of heat flux. This allows the data to be represented well as a single average for the local heat transfer coefficient measurement (using the slope of the regression line) for each type of surface, shown in Fig. 7. In this figure, the data are more clearly represented to demonstrate the local condensation heat transfer coefficient as a function of average powder diameter. With a consistently sized monolayer powder surface, this graphical representation demonstrates the trend in thermal performance for surface roughness from the smallest powder size to the largest powder size. The standard error for this averaged value of the local heat transfer coefficient is used to determine the measurement error. A 23% improvement in the local heat transfer coefficient ($h_l = 183$

Table 1 Copper powder information for each sample tested. A minus sign “-” indicates that the powder passes through that screen mesh while a plus sign “+” indicates that the powder is stopped by that screen mesh size. The advancing and receding contact angle is indicative for each microporous surface.

Powder grade	Average powder diameter (μm)	θ_a (deg)	θ_r (deg)	$\theta_a - \theta_r$ (deg)
Smooth	None	91.0 ± 0.6	83.5 ± 2.7	7.5 ± 2.8
2000	$4 \mu\text{m}$	127.5 ± 2.2	98.0 ± 1.1	29.5 ± 2.5
500 A (-325)	$21 \mu\text{m}$	140.8 ± 2.0	85.0 ± 5.0	55.8 ± 5.4
155 A (-325)	$43 \mu\text{m}$	153.5 ± 1.5	92.5 ± 4.0	61.0 ± 4.9
103 A (-150/+325)	$61 \mu\text{m}$	153.5 ± 1.0	90.5 ± 0.6	63.0 ± 1.2
Cu31 (-80/+150)	$119 \mu\text{m}$	141.8 ± 0.8	116.3 ± 3.1	25.5 ± 3.2

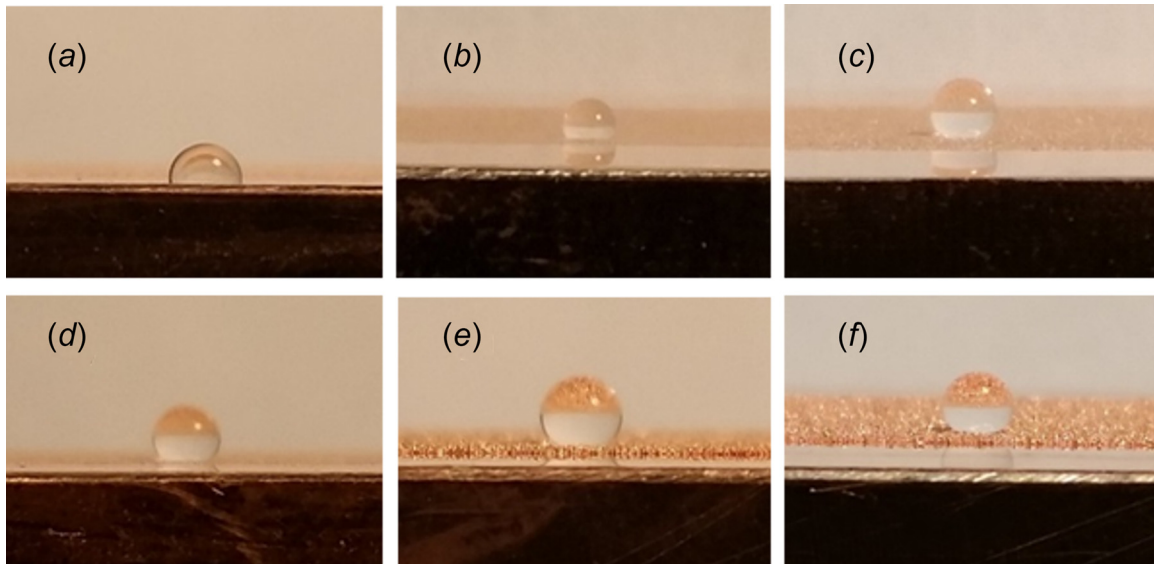


Fig. 5 Water droplets approximately $10.12 \mu\text{L}$ deposited on superhydrophobic microporous copper powder. The average powder diameter used for each sample is (a) none, (b) $4 \mu\text{m}$, (c) $21 \mu\text{m}$, (d) $43 \mu\text{m}$, (e) $61 \mu\text{m}$, and (f) $119 \mu\text{m}$.

$\pm 6 \text{ kW/m}^2 \text{ K}$) is evident for the smallest copper powder size ($4 \mu\text{m}$) compared to a smooth surface. The droplet growth for the $4 \mu\text{m}$ powder sample is likely in the partially wetting mode for a Cassie-state droplet [28]. The partially wetting mode droplet morphology enhances the heat transfer efficiency for Cassie-state droplets due to the ability for vapor to penetrate beneath the wick

structure and directly condense within the wick [29]. To extend the findings of Miljkovic et al., the liquid bridge formed between the copper surface and the droplet growing along the microporous powder is relatively high in thermal conductivity. If this liquid bridge exists, this parallel conduction heat transfer path likely contributes to the enhanced thermal performance observed for the

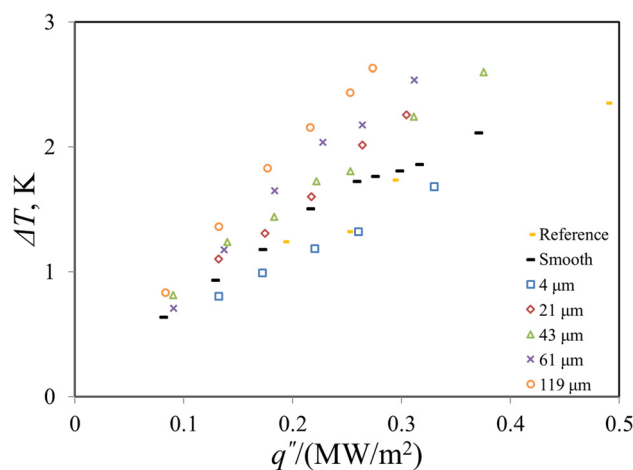


Fig. 6 The local vapor-to-surface temperature difference plotted against the local condensation heat flux is used to analyze the heat transfer efficiency of the superhydrophobic microporous wick structures. Reference data are from Stylianou and Rose [27] for a comparable smooth hydrophobic copper surface.

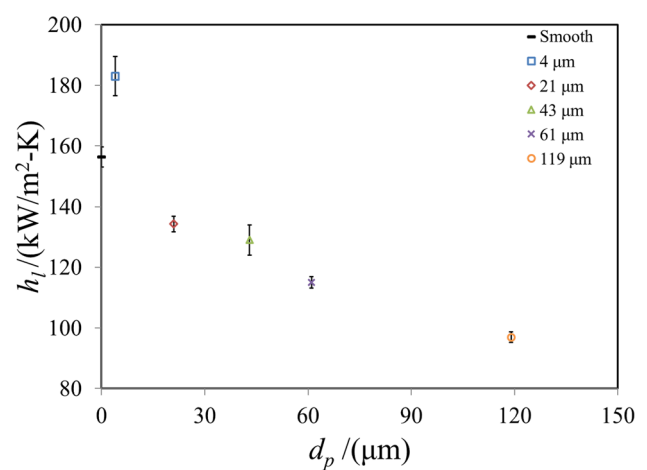


Fig. 7 The heat flux averaged local heat transfer coefficient plotted against copper powder diameter to demonstrate the trend in thermal performance from smallest to largest powder size. The smallest superhydrophobic copper powder ($4 \mu\text{m}$) surface outperforms a smooth hydrophobic surface by 23%.

4 μm powder sample. Additional surface imaging during condensation using environmental scanning electron microscope (ESEM) would demonstrate the true nature of this phenomenon.

The subsequent data for larger powder sizes are progressively worse in thermal performance. This is due to the formation of more highly pinned droplets with high contact angle hysteresis and droplet growth in a mixed wettability mode on the wick structures [17,30]. The increased hysteresis increases the maximum departing droplet size, creating a shift in droplet size distribution toward larger droplets. Evidence of this pinning effect can be seen in Fig. 8 for larger copper powder sizes. The increased average droplet size increases the conduction resistance, leading to decreased heat transfer efficiency. The thermal performance is also worse due to the exhibited mixed wettability mode that is demonstrated by these larger powder size (21 μm diameter and greater) wicked substrates. In this mixed wettability mode, condensation can occur on the liquid film near the top of the wick structure, rather than exclusively within the powder layer as demonstrated with the smaller diameter powders operating in a partially wetted mode [31]. This would lead to an increased liquid conduction resistance in a suspended wetting mode as compared to the case where condensation occurs directly at the base of the wick structure. The results additionally suggest that another transition begins to occur for the largest powder sample (119 μm). It appears that some of the liquid condensing within the wick structure do not collect in the droplets above the wick, but travel as a film beneath the wick [32,33]. It is likely that this powder size is on the cusp of a more extreme transition to decreased thermal performance. The combined effects described above contribute to overall low heat transfer efficiency for all powder sizes excluding the smallest structured realized in this study.

Departing Droplet Size. The high heat transfer efficiency of the smallest copper powder size (4 μm) compared to a smooth copper surface is a significant distinction. Without including the results of the 4 μm powder, the smooth hydrophobic copper surface demonstrates the highest heat transfer coefficients. The relatively high heat transfer coefficients with the smooth surface are

attributed to its relatively low contact angle hysteresis and zero additional conduction resistance. Further observations show that the departing droplet size appears to be the primary variable governing heat transfer, in addition to secondary explanations, such as the droplet growth mode, conduction resistance, and filmwise modes of condensation underneath the powder structures. The maximum departing droplet sizes were measured for several departing droplets located near the top of all of the condensation surfaces. The measurements were acquired using burst shot imaging of the droplets at consistent high heat flux and measuring the droplet sizes digitally immediately before droplet departure. Empirical photo evidence used is comparable to what is shown in Fig. 8. The results of these measurements are plotted in Fig. 9, which shows the measured maximum departing droplet radius as a function of copper powder diameter. The error bars indicate the standard error of the mean for departing droplet sizes measured for five departing droplets over a 3-s interval. Only the 4 μm powder exhibited departing droplet sizes that were smaller than the smooth surface, while all other samples showed larger departing droplet sizes. Figure 10 plots the thermal performance data against the maximum departing droplet radii data. A clear trend showing decreasing heat transfer with increasing departing droplet size is evident, regardless of whether or not the surface is smooth or modified with sintered powder. A power-law relationship exists for the local heat transfer coefficient as a function of departing droplet radius across all surfaces, both smooth and textured, with a value of -0.57 . Here, it is noted that this is consistent with the model developed and correlated by Bonner [34], which indicated a power-law relationship value between $-1/2$ and $-2/3$ for the heat transfer efficiency of the condensation of steam as a function of departing droplet radius.

Interestingly, the departing droplet radii results for the condensation of steam for the smallest (4 μm) and largest (119 μm) powders seem to contradict the contact angle hysteresis measurements acquired in air. The copper powder samples sized 21 μm , 43 μm , and 61 μm all indicate a large contact angle hysteresis in air, as shown in Table 1. The smooth 4 μm , and 119 μm surfaces demonstrate smaller contact angle hysteresis, with the smooth surface generating the smallest value. The results for the condensation of

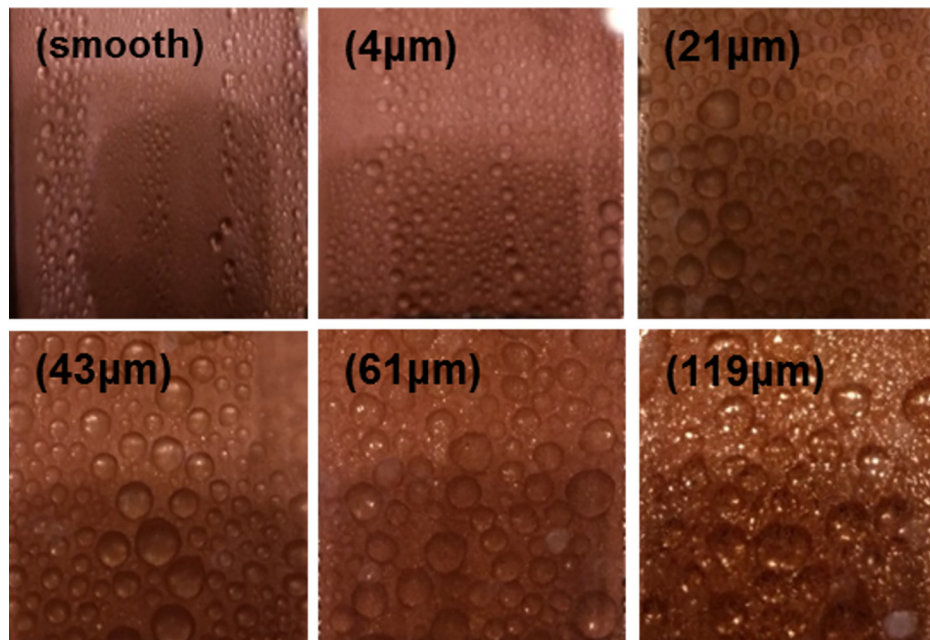


Fig. 8 Droplet growth and coalescence for a smooth, 4 μm , 21 μm , 43 μm , 61 μm , and 119 μm copper powder surface. Highly pinned amorphous droplets with high hysteresis contribute to decreased heat transfer efficiency for larger powder sizes. Small departing droplets with low hysteresis contribute to increased heat transfer efficiency for the smallest powder size.

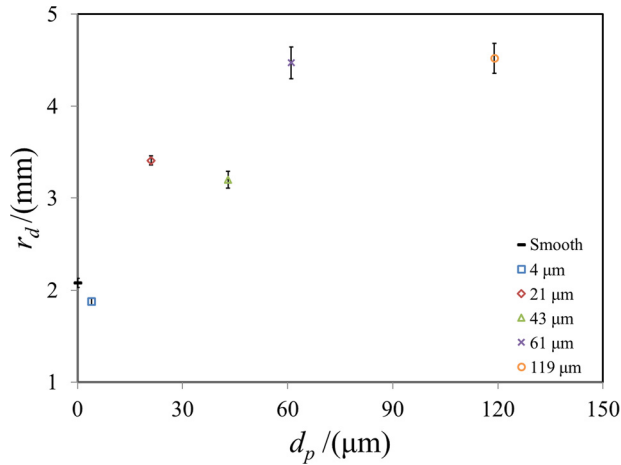


Fig. 9 Maximum departing droplet radius plotted against copper powder diameter. Note that the smallest superhydrophobic copper powder ($4\ \mu\text{m}$) surface has consistently smaller departing droplet radii compared to that on a smooth hydrophobic copper surface.

steam indicate that for the largest powders, there is high contact angle hysteresis under steam conditions resulting in large departing droplets. The $4\ \mu\text{m}$ and smooth surface generate smaller departing droplets with low hysteresis under steam. The contradiction for the $119\ \mu\text{m}$ powder sample is readily explained. Even with a relatively small hysteresis in air, large diameter powder induces a pinning effect during droplet formation under steam conditions, as outlined earlier. This phenomenon creates large departing droplet radii with low thermal performance. The contradiction for the $4\ \mu\text{m}$ powder presents a more valuable result. The hysteresis in air for the $4\ \mu\text{m}$ powder is not smaller than the hysteresis for a smooth surface; however, smaller departing droplet radii result leading to increased thermal performance. Based on this evidence, the contact angle hysteresis in steam conditions for the $4\ \mu\text{m}$ powder has to be smaller than a smooth surface to

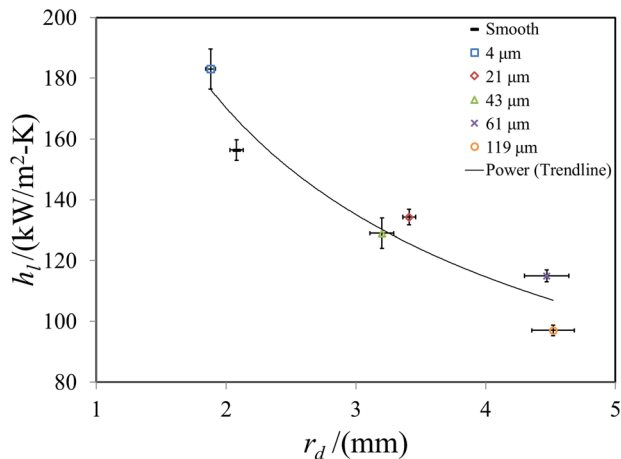


Fig. 10 The heat flux averaged local heat transfer coefficient plotted against maximum departing droplet radius for each surface. This evidence provides further validation to why the smallest superhydrophobic copper powder ($4\ \mu\text{m}$) surface demonstrates better thermal performance than a smooth hydrophobic copper surface. The small departing droplet radii with low hysteresis are efficiently removed from the surface. A power-law relationship exists for the data with a value of -0.574 . This is consistent with the findings from the Bonner correlation [34], which indicated a power-law relationship value between $-1/2$ and $-2/3$ for the condensation of steam. The trendline equation is: $h_l = 253r_d^{-0.57}$.

generate smaller departing droplet radii. Without ESEM to confirm, this is evidenced qualitatively through Fig. 8. This general contradiction was outlined quantitatively by Enright et al. to place the phenomenon into a mechanistic framework. The advantageous wetting states for small length scales of textured surfaces were explained by local contact line depinning behavior during droplet coalescence [35]. It is clear that the most desirable surfaces for dropwise condensation would have the low hysteresis of a smooth surface under steam conditions with little conduction resistance, possibly through textured surface modification. Generally, the hysteresis in air may not translate well to steam condensation conditions. In essence, a superhydrophobic $4\ \mu\text{m}$ copper powder surface emulates the effect of a smooth hydrophobic surface but with more advantageous droplet shedding properties.

Conclusion

Superhydrophobic surfaces were developed using self-assembled monolayers deposited on microporous copper powder wick structures, which are commonly and cost effectively used in heat pipe manufacturing. The local heat transfer coefficient for dropwise condensation of steam on these surfaces was then experimentally measured. As a result, local heat transfer coefficients for the larger powder surfaces ($21\ \mu\text{m}$ diameter and greater) were lower than local heat transfer coefficients obtained on a smooth copper surface. Competing factors influence the decreased thermal efficiency observed. The formation of strongly pinned droplets led to a shift in the departing droplet size distribution toward larger sizes. The large departing droplet radii and secondarily additional conduction resistance both contributed to decreased thermal performance. The smallest microporous copper powder structure ($4\ \mu\text{m}$) demonstrated a 23% improvement in the local heat transfer coefficient compared to a smooth copper surface. The partially wetting droplet growth mode for the $4\ \mu\text{m}$ powder sample, as opposed to a mixed wettability mode, contributed to enhanced heat transfer efficiency. A clear trend was identified where heat transfer coefficients correlated strongly with the maximum departing droplet size for both smooth and sintered powder coated surfaces. The correlation between heat transfer and departing droplet size that was identified is also consistent with other correlations developed for multiple fluids on smooth surfaces. Interestingly, the contact angle hysteresis observed with sessile water droplets in air did not lead to smaller departing droplet sizes for small powder sizes when condensing in a saturated steam environment. The use of smaller diameter nanostructures that do not rely on trapped noncondensable gas (such as air) to promote lower hysteresis may be better suited for improving thermal performance than microporous powders alone. The design of hydrophobic porous surfaces could lead to more efficient two-phase thermal management at high heat flux if smaller departing droplet sizes under saturated steam conditions can be realized.

Acknowledgment

The authors would like to thank Phil Martin and Maksym Demydovych for their experimental design and testing expertise, as well as Professor Massoud Kaviany and Minki Kim from the University of Michigan for the sample SEM images.

Funding Data

- This work was funded by the Office of Science in the U.S. Department of Energy (DOE) under a Phase II SBIR grant (Award No. DE-SC-0011317). The program manager was Robie Lewis.

Nomenclature

d_p = average copper powder diameter
 (dT/dx) = temperature gradient with respect to path length
 h_l = local heat transfer coefficient

k_s = substrate thermal conductivity
 q'' = heat flux through condensing surface
 r_d = maximum departing droplet radius
 T_s = surface temperature
 T_v = vapor temperature at saturation pressure
 x = path length through test block
 ΔT = difference between vapor and surface temperature

References

- [1] Bonner, R. W., III, 2010, "Dropwise Condensation in Vapor Chambers," 26th Annual IEEE Semiconductor Thermal Measurement and Management Symposium (SEMI-THERM), Santa Clara, CA, Feb. 21–25.
- [2] Schmidt, E., Schurig, W., and Sellschopp, W., 1930, "Versuche Über Die Kondensation in Film- Und Tropfenform," *Tech. Mech. Thermodyn.*, 1(2), pp. 55–63.
- [3] Bonner, R., III, 2011, "Dropwise Condensation Life Testing of Self-Assembled Monolayers," *ASME* Paper No. IHTC14-22936.
- [4] Rose, J., 2002, "Dropwise Condensation Theory and Experiment: A Review," *Proc. Inst. Mech. Eng. Part A*, **216**(2), pp. 115–128.
- [5] Bonner, R. W., III, 2009, "Dropwise Condensation on Surfaces With Graded Hydrophobicity," *ASME* Paper No. HT2009-88516.
- [6] Patankar, N. A., 2004, "Mimicking the Lotus Effect: Influence of Double Roughness Structures and Slender Pillars," *Langmuir*, **20**(19), pp. 8209–8213.
- [7] Patankar, N. A., 2010, "Supernucleating Surfaces for Nucleate Boiling and Dropwise Condensation Heat Transfer," *Soft Matter*, **6**(8), pp. 1613–1620.
- [8] Kim, S., and Kim, K. J., 2011, "Dropwise Condensation Modeling Suitable for Superhydrophobic Surfaces," *ASME J. Heat Transfer*, **133**(8), p. 081502.
- [9] Mendoza, H., Beaini, S., and Carey, V. P., 2011, "An Exploration of Transport Within Micro and Nano Droplet Clusters During Dropwise Condensation of Water on Nanostructured Surfaces," *ASME* Paper No. IMECE2011-64151.
- [10] Beaini, S. S., Mendoza, H., and Carey, V. P., 2012, "The Effect of Thermal Resistance for Dropwise Condensation on Hydrophobic Micro-Pillared Structures," *ASME* Paper No. IMECE2012-89574.
- [11] Dietz, C., Rykaczewski, K., Fedorov, A. G., and Joshi, Y., 2010, "Visualizations of Droplet Departure on a Superhydrophobic Surface and Implications to Heat Transfer Enhancement During Dropwise Condensation," *Appl. Phys. Lett.*, **97**, p. 033104.
- [12] Rykaczewski, K., Osborn, W. A., Chinn, J., Walker, M. L., Scott, J. H. J., Jones, W., Hao, C., Yao, S., and Wang, Z., 2012, "How Nanorough Is Rough Enough to Make a Surface Superhydrophobic During Water Condensation?," *Soft Matter*, **8**(33), p. 8786.
- [13] Rykaczewski, K., Scott, J. H. J., Rajauria, S., Chinn, J., Chinn, A. M., and Jones, W., 2011, "Three Dimensional Aspects of Droplet Coalescence During Dropwise Condensation on Superhydrophobic Surfaces," *Soft Matter*, **7**(19), p. 8749.
- [14] Rykaczewski, K., Paxson, A. T., Anand, S., Chen, X., Wang, Z., and Varanasi, K. K., 2013, "Multimode Multidrop Serial Coalescence Effects During Condensation on Hierarchical Superhydrophobic Surfaces," *Langmuir*, **29**(3), pp. 881–891.
- [15] Rykaczewski, K., 2012, "Microdroplet Growth Mechanism During Water Condensation on Superhydrophobic Surfaces," *Langmuir*, **28**(20), pp. 7720–7729.
- [16] He, B., Patankar, N. A., and Lee, J., 2003, "Multiple Equilibrium Droplet Shapes and Design Criterion for Rough Hydrophobic Surfaces," *Langmuir*, **19**(12), pp. 4999–5003.
- [17] Narhe, R. D., and Beysens, D. A., 2007, "Growth Dynamics of Water Drops on a Square-Pattern Rough Hydrophobic Surface," *Langmuir*, **23**(12), pp. 6486–6489.
- [18] Narhe, R. D., and Beysens, D. A., 2004, "Nucleation and Growth on a Superhydrophobic Grooved Surface," *Phys. Rev. Lett.*, **93**(7), p. 076103.
- [19] Chen, C.-H., Cai, Q., Tsai, C., Chen, C.-L., Xiong, G., Yu, Y., and Ren, Z., 2007, "Dropwise Condensation on Superhydrophobic Surfaces With Two-Tier Roughness," *Appl. Phys. Lett.*, **90**(17), p. 173108.
- [20] Zheng, Y., Chen, C.-H., Pearlman, H., Flannery, M., and Bonner, R., 2015, "Effect of Porous Coating on Condensation Heat Transfer," *Ninth International Conference on Boiling and Condensation Heat Transfer*, Boulder, CO, Apr. 26–30.
- [21] Zheng, Y., Chen, C.-H., Pearlman, H., and Bonner, R., 2016, "Enhanced Filmwise Condensation With Thin Porous Coating," First Pacific Rim Thermal Engineering Conference (PRTEC), Big Island, HI, Paper No. PRTEC-14728.
- [22] Faghri, A., 1995, *Heat Pipe Science and Technology*, Taylor & Francis, Washington, DC.
- [23] Hwang, G. S., Kaviany, M., Anderson, W. G., and Zuo, J., 2007, "Modulated Wick Heat Pipe," *Int. J. Heat Mass Transfer*, **50**(7–8), pp. 1420–1434.
- [24] Hwang, G. S., Fleming, E., Carne, B., Sharratt, S., Nam, Y., Dussinger, P., Ju, Y. S., and Kaviany, M., 2011, "Multi-Artery Heat-Pipe Spreader: Lateral Liquid Supply," *Int. J. Heat Mass Transfer*, **54**(11–12), pp. 2334–2340.
- [25] Hwang, G. S., Nam, Y., Fleming, E., Dussinger, P., Ju, Y. S., and Kaviany, M., 2010, "Multi-Artery Heat Pipe Spreader: Experiment," *Int. J. Heat Mass Transfer*, **53**(13–14), pp. 2662–2669.
- [26] Anderson, D. M., Gupta, M. K., Voevodin, A. A., Hunter, C. N., Putnam, S. A., Tsukruk, V. V., and Fedorov, A. G., 2012, "Using Amphiphilic Nanostructures to Enable Long-Range Ensemble Coalescence and Surface Rejuvenation in Dropwise Condensation," *ACS Nano*, **6**(4), pp. 3262–3268.
- [27] Stylianou, S., and Rose, J., 1980, "Dropwise Condensation on Surfaces Having Different Thermal Conductivities," *ASME J. Heat Transfer*, **102**(3), pp. 477–482.
- [28] Cho, H. J., Preston, D. J., Zhu, Y., and Wang, E. N., 2016, "Nanoengineered Materials for Liquid-Vapour Phase-Change Heat Transfer," *Nat. Rev. Mater.*, **2**, p. 16092.
- [29] Miljkovic, N., Enright, R., and Wang, E. N., 2012, "Effect of Droplet Morphology on Growth Dynamics and Heat Transfer During Condensation on Superhydrophobic Nanostructured Surfaces," *ACS Nano*, **6**(2), pp. 1776–1785.
- [30] Miljkovic, N., Enright, R., Nam, Y., Lopez, K., Dou, N., Sack, J., and Wang, E. N., 2013, "Jumping-Droplet-Enhanced Condensation on Scalable Superhydrophobic Nanostructured Surfaces," *Nano Lett.*, **13**(1), pp. 179–187.
- [31] Miljkovic, N., Enright, R., and Wang, E. N., 2013, "Condensation Heat Transfer on Superhydrophobic Surfaces," *MRS Bull.*, **38**(5), pp. 397–406.
- [32] Wier, K. A., and McCarthy, T. J., 2006, "Condensation on Ultrahydrophobic Surfaces and Its Effect on Droplet Mobility: Ultrahydrophobic Surfaces Are Not Always Water Repellent," *Langmuir*, **22**(6), pp. 2433–2436.
- [33] Cheng, J., Vandadi, A., and Chen, C.-L., 2012, "Condensation Heat Transfer on Two-Tier Superhydrophobic Surfaces," *Appl. Phys. Lett.*, **101**, p. 131909.
- [34] Bonner, R. W., III, 2013, "Correlation for Dropwise Condensation Heat Transfer: Water, Organic Fluids, and Inclination," *Int. J. Heat Mass Transfer*, **61**, pp. 245–253.
- [35] Enright, R., Miljkovic, N., Al-Obeidi, A., Thompson, C. V., and Wang, E., 2012, "Condensation on Superhydrophobic Surfaces: The Role of Local Energy Barriers and Structure Length Scale," *Langmuir*, **28**(40), pp. 14424–14432.